Near-critical phase explosion promoting breakdown plasma ignition during laser ablation of graphite

A. A. Ionin, S. I. Kudryashov,* and L. V. Seleznev
P.N. Lebedev Physical Institute, Russian Academy of Sciences, 119991 Moscow, Russia
(Received 10 March 2010; published 16 July 2010)

Removal rate, air shock, and ablative recoil pressure parameters were measured as a function of laser intensity I_{peak} during nanosecond laser ablation of graphite. Surface vaporization of molten graphite at low intensities $I_{peak}<0.15$ GW/cm^2 was observed to transform into its near-critical phase explosion (intense homogeneous boiling) at the threshold intensity $I_{PE}\approx 0.15$ GW/cm^2 in the form of a drastic, correlated rise of removal rate, air shock, and ablative recoil pressure magnitudes. Just above this threshold ($I_{peak}\geq 0.25$ GW/cm^2), the explosive mass removal ended up with saturation of the removal rate, much slower increase of the air and recoil pressure magnitudes, and appearance of a visible surface plasma spark. In this regime, the measured far-field air shock pressure amplitude exhibits a sublinear dependence on laser intensity ($\propto I_{peak}^{4/9}$), while the source plasma shock pressure demonstrates a sublinear trend ($\propto I_{peak}^{3/4}$), both indicating the subcritical character of the plasma. Against expectations, in this regime the plasma recoil pressure increases versus I_{peak} superlinearly ($\propto I_{peak}^{1.1}$), rather than sublinearly ($\propto I_{peak}^{3/4}$), with the mentioned difference related to the intensity-dependent initial spatial plasma dimensions within the laser waist on the graphite surface and to the plasma formation time during the heating laser pulse (overall, the pressure source effect). The strict coincidence of the phase explosion, providing high (kbar) hydrodynamic pressures of ablation products, and the ignition of ablative laser plasma in the carbon plume may indicate the ablative pressure-dependent character of the underlying optical breakdown at the high plume pressures, initiating the plasma formation. The experimental data evidence that the spatiotemporal extension of the plasma in the laser plume and ambient air during the heating laser pulse is supported by fast lateral electron and radiative heat conduction (laser-supported combustion wave regime), rather than by propagation of a strong shock wave (laser-supported detonation wave regime).

DOI: 10.1103/PhysRevE.82.016404 PACS number(s): 52.38.Mf, 52.50.Jm, 52.35.Tc, 64.70.F−

I. INTRODUCTION

High-power laser irradiation of materials surfaces usually results in intense vaporization of a laser-superheated surface molten layer and its following intense homogeneous boiling (phase explosion) at near-critical temperatures $T\leq T_{cr}$ [1–4]. However, if the vaporized atoms and molecules possess low first ionization potentials J_p (i.e., $J_p/k_BT_{cr}<1$, where k_B is the Boltzmann constant), laser-induced optical breakdown and plasma ignition may occur in the vapor during surface vaporization, i.e., prior the phase explosion [5]. In contrast, in the other case of $J_p/k_BT_{cr}>1$, such phase explosion at $T\leq T_{cr}$ precedes optical breakdown and plasma ignition in the ablation plume [6]. The relationship between the near-critical phase explosion and plasma formation, or, in other words, the order of their appearance on a laser intensity scale, is very important for multiple applications, such as laser-induced breakdown spectroscopy (LIBS) in laser plumes [6], inductively coupled plasma sources for mass-spectrometric, atomic emission and other analytical techniques equipped with laser microsampling [7,8]. In particular, such sequence of phase explosion and plasma formation dictates a composition of primary gaseous products (vapor, vapor/droplet mixture, plasma) of laser ablation and basic parameters of the resulting plasmas.

Interestingly, since the 70s, when this important phenomenological criterion based on the ratio J_p/k_BT_{cr} has been derived via a broad overview of the large set of experimental facts [5], representing well-defined plasma formation thresholds during pulsed laser ablation [9], it was neither verified in any independent experiments, nor tested by theory. Furthermore, no any other advanced relevant criteria, relating ablative mass removal and laser plasma ignition in ablation plumes were proposed since that time. Meanwhile, this criterion obviously ignores essential monotonous laser wavelength [4,10,11] and nonmonotonous vapor pressure effects [4,11] on an onset of optical breakdown in laser plumes prior plasma formation, which determine basic relationships between local (optical breakdown) and non-local (plasma absorption and screening) optical effects, and corresponding spatiotemporal dynamics in a near-surface "opaqueness" region [12] during ignition of the laser ablative plasma. Such very early (ignition) stage of laser ablative plasma dynamics, relating together ablative mass removal and plasma phenomena, is crucial for understanding of emissive, hydrodynamic and energetic characteristics of the hot and dense plasma core region in laser plumes, and of a stochastic, strongly perturbative spatial structure of the plasma in the near-surface "opaqueness" region [12]. Nevertheless, so far there were only a limited number of experimental studies covering mass removal, onset and development of plasma during high-power laser ablation [13–17], as compared to multiple experimental and theoretical research works on mechanical coupling (vapor/plasma recoil momentum transfer) to laser-ablated targets, relating together characteristic intensity values for the maximum of mechanical impulse coupling coef-

*Corresponding author; sikudr@sci.lebedev.ru

ficient C_m, optical breakdown in corresponding ablative plumes and subsequent plasma extension via laser-supported combustion wave [1,18–20]. As a result, the relationships between the mass removal, vapor gasdynamic, or plasma hydrodynamic flow, and ionization phenomena during high-power laser ablation are remaining unexplored in details. As an example, it is not widely accepted yet whether laser plasma formation in ablation plumes occurs via rather gradual heating of an expanding vapor through the inverse Bremsstrahlung absorption mechanism [16,21,22], or such plasma may appear suddenly in the plume during laser ablation above some threshold intensity value [1,4–6,9–11], which simultaneously provides sufficient pressure of the target vapor and its pressure-dependent optical breakdown. Also, it is interesting to study characteristics of optical breakdown at high (kbar) vapor pressures typical for laser ablative plumes, but hardly accessible at stationary compression of gases [19].

In this work we experimentally demonstrate a strict correlation between a thresholdlike nanosecond laser-induced phase explosion on graphite surface, providing high removal rates and high (kbar) hydrodynamic pressures in the resulting ablation plumes, and the following formation of an ablative subcritical plasma. These experimental studies and related modeling show that this sequence of the phase explosion and optical breakdown (plasma ignition) in the plumes is dictated by the vapor pressure dependence of the breakdown threshold, revealing interesting spatiotemporal dynamics of the optical breakdown, plasma formation, and extension during the laser ablation of graphite.

II. EXPERIMENTAL SETUP AND TECHNIQUES

In these experiments we performed laser ablation of millimeter-thick polycrystalline graphite plates (mass density $\rho_0 \approx 1.7$ g/cm^3). A primary laser source was a frequency-doubled Nd:YAG laser (LTIPCh-412) with a lasing wavelength $\lambda_{las} \approx 532$ nm, laser pulse full width at a half maximum (FWHM) $\tau_{las} \approx 25$ ns, and a maximum pulse energy in the TEM_{00} mode ≈ 50 mJ at a repetition rate of 12.5 Hz. The 532 nm laser pulses were focused using a silica lens (focal length $f \approx 40$ cm) into focal spots $w_0 \approx 40-150$ μm (at the $1/e$ level) and their energies were monitored by means of a thermocouple energy meter (Fig. 1).

Contact ultrasonic measurements of ablative pressure were carried out in a single-shot mode at variable peak laser intensities $I_{peak}=0.1-2$ GW/cm^2 in the acoustic far-field region using a brass-disk protected piezoelectric transducer ($LiNbO_3$, the effective bandwidth <20 MHz, sensitivity of 1 mV/atm) [23,24], with the graphite plate sliding on the 3mm thick protective front cover brass disk of the transducer via a thin lubricating vacuum grease layer. The active front electrode of the transducer was centered relative to the laser focal point on the front surface of the sample. The acquired ultrasonic transients with the first compressive (P_{comp}) and the second rarefaction (P_{rare}) pressure pulses were bipolar ($P_{comp} > P_{rare}$) at lower laser intensities $I_{peak} < 0.15$ GW/cm^2 and almost unipolar ($P_{comp} \gg P_{rare}, P_{rare} \approx 0$) at higher I_{peak} values, representing a superposition of

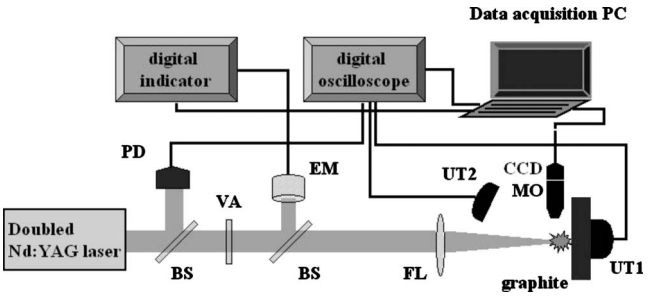

FIG. 1. Experimental setup for ultrasonic studies during 532-nm nanosecond laser ablation of graphite: BS—beam splitter, PD—fast trigger silicon photodiode, VA—variable energy attenuator, FL—focusing silica lens, EM—thermocouple energy meter, UT1,2—ultrasonic transducers for rear-side solid and front-side air measurements, MO and CCD—microscope objective equipped by CCD camera, PC—laptop computer for data acquisition.

bipolar thermoacoustic ($\propto dI/dt$) and unipolar vapor (plasma) recoil ($\propto I(t)$) pressure signals [24,25]. The resulting vapor or plasma recoil pressures were then derived as follows [24,25]

$$P_{rec} = \frac{(P_{comp} - P_{rare})}{2} \quad \text{(bipolar transients)}, \tag{1a}$$

$$P_{rec} \approx P_{comp} \quad \text{(unipolar transients)}. \tag{1b}$$

Also, we performed non-contact ultrasonic measurements of air transit times (t_{tr}) and compressive pressure amplitudes (P_{air}) versus $I_{peak}=0.01-50$ GW/cm^2 for sonic and supersonic (shock) waves, driven in air during the simultaneous laser ablation of the graphite samples, placing a piezoelectric transducer Miniwat-2 (PVDF, bandwidth <30 MHz, sensitivity of 10 V/atm, UC VINFIN) [26] at the far-field distance $l_{air} \approx 23$ mm in front of the samples. The voltage transients from the transducers were recorded using a 50-Ω input of a digital storage oscilloscope Tektronix TDS-2024, which was triggered via another 50-Ω input by an electric pulse from a fast photodiode DET-210 (Thorlabs) fed by a weak split laser beam.

Similarly, average removal rates X per laser shot at different I_{peak} values were ultrasonically measured for the graphite, acquiring average intensity-dependent temporal displacements of the corresponding ultrasonic pulse fronts per each shot to the smaller transit times, driven by extension of the ablation craters through the graphite plate to the ultrasonic transducer on its rear side, and multiplying the acquired average displacement per shot by the longitudinal sound velocity [27] in the graphite sample $C_{l,grap} \approx 2.3$ km/s. The latter value was experimentally measured, detecting ultrasonic transit times for a few polycrystalline graphite plates of different thickness.

III. EXPERIMENTAL RESULTS

A. Surface phase explosion

At low incident peak laser intensities $I_{peak} \leq 0.15$ GW/cm^2 the measured low removal rate X and recoil pressure P_{rec} vary super-linearly ($\propto I_{peak}^{1.3}$) before the next

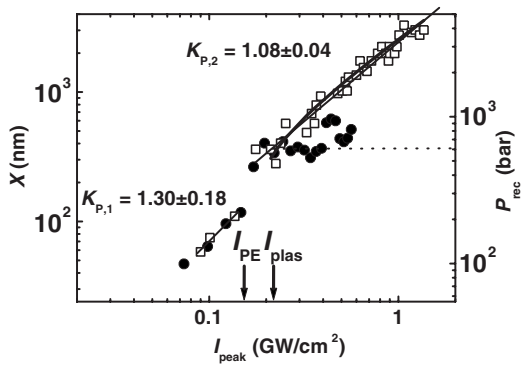

FIG. 2. Average removal rate X (dark circles, left axis) and calibrated recoil pressure P_{rec} in bars (light squares, right axis) for the polycrystalline graphite versus peak laser intensity I_{peak} with the arrows and marks I_{PE}, I_{plas} denoting the phase explosion and plasma formation thresholds, respectively. The straight thin lines denote their linear fitting curves with power slopes $K_{P,1}=1.30\pm0.18$ (for $I_{peak}<I_{PE}$) and $K_{P,2}=1.08\pm0.04$ (for $I_{peak}>I_{plas}$), as well as the special fitting curve $I_{peak}^{3/4}\{\ln[I_{peak}/I_{plas}]\}^{1/2}$ (the upper thick one at high I_{peak}). The horizontal dotted line denotes the maximum ablation pressure value of ≈620 bar achieved at $I_{peak}\approx I_{plas}$ prior dense plasma formation.

sharp increase (Fig. 2), correlating to each other and corresponding to the common surface vaporization regime (vaporization front velocity $V_{ev}\sim X/\tau_{las}\sim 1-10$ m/s) [2–4,28]. The superlinear $X(I_{peak})$ dependence, contradicting, at the first glance, to previous theoretical predictions ($V_{ev}\propto I_{peak}$ [2,4]), can be nevertheless expressed in the linear form $X\propto(I_{peak}-I_{abl})^{0.97\pm0.09}$, where the vaporization threshold $I_{abl}\approx0.03$ GW/cm^2 for the polycrystalline graphite is consistent with the nanosecond laser melting threshold for highly-oriented pyrolitic graphite (HOPG) ≈0.02 GW/cm^2 [24,29], as graphite melting is known to be accompanied by intense vaporization of its molten phase [24,30,31] (the extrapolated $P_{rec}\sim10$ bar at $I_{abl}\approx0.03$ GW/cm^2 in Fig. 2; see also similar extrapolated value $P_S\approx20$ bar at $I_{abl}\approx0.03$ GW/cm^2 in Fig. 5 below, while note that the equilibrium vapor pressure could be higher by the factor of 2 because of the unidirectional (off the surface) character of the nonequilibrium vapor flow [4,28]).

The good correlation between the integral X and instantaneous (peak) P_{rec} magnitudes may mean that the surface vaporization occurs in a steady-state manner over the incident laser pulse, and can be used to estimate absolute values of the measured recoil pressures. For this purpose, the known hydrodynamic continuity relations (mass and momentum conservation rules) [4,28] can be employed in the form

$$\rho_0 V_{ev}\approx\rho_{vap}V_{vap}, \tag{2a}$$

$$\rho_0 V_{ev}V_{vap}\approx\rho_{vap}V_{vap}^2, \tag{2b}$$

where the vapor recoil pressure $P_{rec}\approx\rho_0 V_{ev}V_{vap}$ is determined by the removal rate ($V_{ev}\sim X/\tau_{las}$) and lift-off velocity $V_{vap}\approx(RT/M)^{1/2}\approx2.1\times10^3$ m/s of the predominant vaporized carbon species C_1 [30] with the molar mass $M_1=1.2\times10^{-2}$ kg/mole at the near-critical surface temperature $T\approx T_{cr}\approx7\times10^3$ K [30,31]. The estimated ablative recoil pressures $P_{rec}\sim10^2$ in Fig. 2 are in semiquantitative agreement with the equilibrium saturated vapor pressure values at the near-critical temperatures $T\leq T_{cr}$ [31], accounting for the unidirectional character of the vapor flow.

Then, the following drastic correlated increase of the $X(I_{peak})$ and $P_{rec}(I_{peak})$ curves at $I_{peak}\geq0.15$ GW/cm^2 in Fig. 2 can be related to laser-induced surface phase explosion in the vicinity of the critical point of carbon at the intensity threshold I_{PE}. This assumption is supported by our estimates of the maximum ablative recoil pressure $P_{rec}\sim10^3$ bar (Fig. 2) achieved prior an onset of optical vapor breakdown at $I_{plas}\approx0.25$ GW/cm^2 (see Secs. III B and IV below), which is consistent, accounting for the abovementioned unidirectional character of the vapor flow [4,28], with the critical pressure of carbon $P_{cr}\approx2230$ bar [30,31]. The persisting good qualitative correlation for $I_{peak}\geq I_{PE}$ between X and P_{rec} magnitudes related by Eqs. (2a) and (2b) via V_{ev}, indicates that the magnitude V_{vap} remains almost constant during the heating laser pulse in this ablation regime (the same appears to be true for the temperature in the near-surface melt layer), but the removal rate strongly increases under the near-critical conditions, representing an onset of the surface phase explosion, which may occur as a superposition of consequent processes of intense and quasi-continuous surface vaporization, bulk homogeneous boiling or even spinodal decomposition of the strongly superheated surface melt [31–33]. More exactly, the liquid/vapor spinodal curve limiting the thermodynamic existence region of the metastable superheated liquid phase was demonstrated to be unattainable under ultrashort pulsed heating [34], while for longer—nanosecond—heating pulses laser-superheated liquids may closely approach this limit [35]. In contrast, surface vaporization path appears to be very arbitrary in the proximity of the spinode curve as the liquid/vapor surface becomes strongly corrugated by vapor bubbles released via the competing bulk boiling process [32] and mean free paths of vapor particles become of the order of inter-particle distances in such dense near-critical vapors. Hence, the intermediate—near-critical homogeneous boiling—process appears to be the most probable ablative mass removal mechanism under circumstances of this study.

Simultaneously, the related dependence $P_{air}(I_{peak})$ also exhibits the same initial region of a non-linear pressure variation prior its succeeding sharp rise near the same intensity value $I_{PE}\approx0.15$ GW/cm^2 (Fig. 3). Meanwhile, in this intensity range the experimentally measured air transit times t_{tr} for the pressure perturbations in air show supersonic average propagation velocities C_{ave} (in air, the sound velocity equals to 0.346 km/s at the normal conditions [36]) (Fig. 4), calculated simply dividing the 23-mm long propagation distance l_{air} by t_{tr}: $C_{ave}=l_{air}/t_{tr}$. In the far-field air region, where the ultrasonic data acquisition takes place, the air pressure perturbations propagate in the form of a spherical (diffracted) wave with the initial radius R_S, which is proportional to the waist radius (see the similarity of P_{air}/w_0 dependences on I_{peak} for $I_{peak}=0.2-50$ GW/cm^2 and different laser spot radii w_0 in inset to Fig. 3), and the almost hyperbolic radial pressure variation [37]

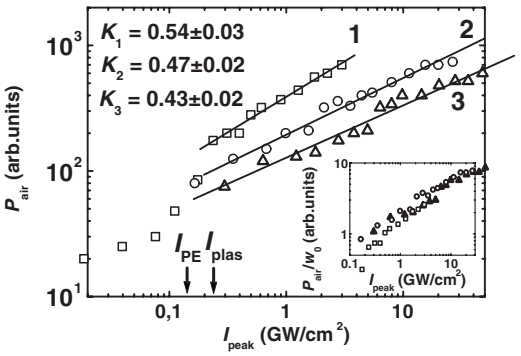

FIG. 3. Air pressure P_{air} for the different laser spot radii w_0 [150 (squares), 55 (circles) and 40 (triangles) μm] versus I_{peak} with the linear fitting curves 1–3 (slopes $K_{1,2,3}$). Inset: the same, but normalized P_{air}/w_0 curves versus I_{peak}.

$$P(r) = P_S\left(\frac{R_S}{r}\right), \tag{3}$$

where P_S is the initial (source) pressure. According to the pressure dependence of the longitudinal sound velocity in air C_{air} [36] (Fig. 4, inset), such diffraction results in gradually decelerating radial motion of the pressure waves from the ablative source on the graphite surface and resulting in the supersonic average propagation velocities C_{ave} reading as

$$C_{ave} = l_{air}\left\{\int_0^{lair} \frac{dr}{C_{air}[P(r)]}\right\}^{-1}. \tag{4}$$

Hence, the measured average propagation velocities C_{ave} in air can be converted into the initial ablative source pressures P_S and shock wave velocities C_S. The resulting dependence $P_S(I_{peak})$ in Fig. 5 demonstrates drastic rise at $I_{peak} \geq I_{PE}$, as well as the related $X(I_{peak})$ and $P_{rec}(I_{peak})$ curves, with the evaluated ablative pressure values P_S in reasonable agreement with the independently estimated pressure values P_{rec} (Fig. 2); the discrepancy by the factor of 2 may result from redeposition of the ablated material, significantly decreasing its removal rate [38]. The derived P_S magnitudes at $I_{peak} \approx I_{PE}$ are close to the near-critical vapor pressure values of graphite (Fig. 5), as well as similar (a few kbar) ablative

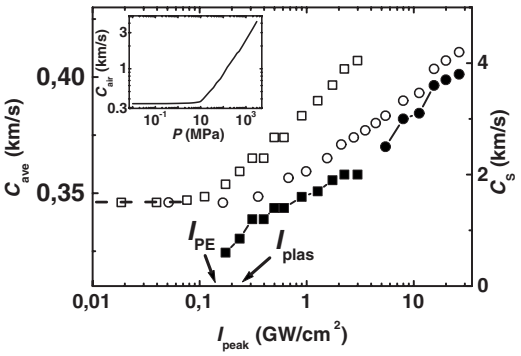

FIG. 4. Average (light marks, C_{ave}, left axis) and initial (dark marks, C_S, right axis) for the different laser spot radii w_0 [150 (squares) and 55 (circles) μm] versus I_{peak}. Inset: pressure dependence of sound velocity in air (after [36]).

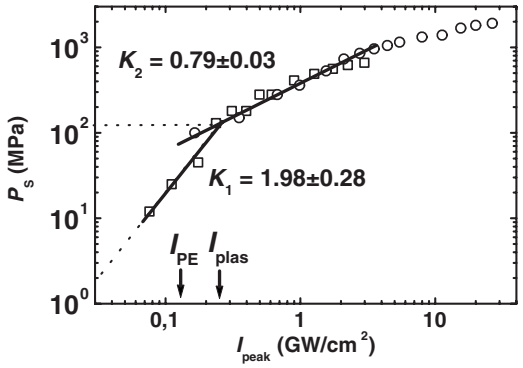

FIG. 5. Plume/plasma pressure P_S for w_0=270 (squares) and 95 (circles) μm versus I_{peak} with the low-($I_{peak} < I_{PE}$) and high-intensity ($I_{peak} > I_{plas}$) linear fitting curves 1–2 (slopes $K_{1,2}$). The dotted horizontal and inclined lines denote the maximum ablation pressure value of $\approx$1140 bar achieved at $I_{peak} \approx I_{plas}$ prior dense plasma formation, and the estimate of the carbon vapor pressure upon its laser melting at $I_{peak} \approx I_{abl} \approx 0.03$ GW/cm^2, respectively.

pressures of aluminum near its laser-induced phase explosion threshold [38], indicating the onset of the near-critical surface phase explosion. In agreement with the unidirectional ablative vapor flow [4,28], the maximum P_S value approaches $0.5P_{cr} \approx 1.1$ kbar at $I_{peak} \approx I_{plas}$, where the rising $P_S(I_{peak})$ curve breaks because of optical breakdown. Likewise, the initial velocity value of the air shock wave in the plume $C_S \approx 1.4$ km/s at $I_{peak} \approx I_{plas}$ (Fig. 4) is also in qualitative agreement with that one near the phase explosion threshold in aluminum ($C_S \approx 5$ km/s) [38].

B. Optical breakdown and plasma formation

Interestingly, at higher laser intensities 0.25 GW/cm^2 $< I_{peak} <$ 0.6 GW/cm^2 the removal rate X saturates at the monotonously increasing P_{rec} (Fig. 2) and P_S (Fig. 5) pressures, i.e., the abovementioned correlation between the mass removal and near-surface plume/plasma pressure quantities fails. The saturation of X indicates that laser ablation is completely screened (shielded) by absorption in the dense ablative plume, while this absorption produces an extra pressure of the plume on the target, which may originate from an expanding ablative laser plasma, emerging in the plume at $I_{peak} \geq 0.3$ GW/cm^2 $> I_{PE}$ [Fig. 6(b)]. By the way, on this and previous images [Figs. 6(a) and 6(b)], corresponding to $I_{peak} \geq I_{PE}$, light tracks (fountains) of micrometer-sized droplets are visible in the laser plumes after the preceding surface phase explosions.

The suggestion on emerging ablative laser plasma is strongly supported by our ultrasonic measurements in air. First, all $P_{air}(I_{peak})$ curves in Fig. 3 for the different focusing conditions—w_0=40, 55, and 150 μm—are well fitted in the range of 0.2–30 GW/cm^2 by a square root dependence, which for the corresponding laser-driven shock waves indicates a square root dependence of source energy density [39]. This functional form is consistent with that of nanosecond laser-heated sub-critical plasma with the plasma energy density and temperature increasing as $\propto I_{peak}^{4/9}$ [40] or, according to other references, as $\propto I_{peak}^{1/2}$ [21,22]. Second, the derived

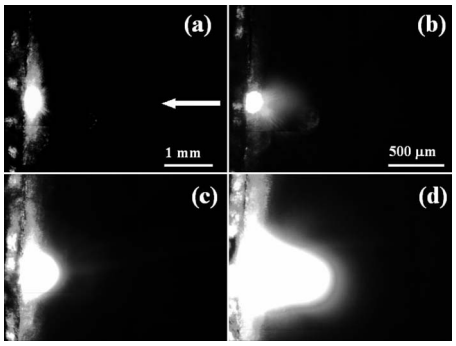

FIG. 6. Optical images of single-shot ablative carbon plasmas at $I_{peak} \approx 0.15$ (a), 0.3 (b), 4 (c) and 14 (d) GW/cm^2 [the scale bar is similar for images (b)–(d)]. The arrow shows the laser incidence direction.

$P_S(I_{peak})$ dependence demonstrates in the range of 0.25–4 GW/cm^2 the scaling relationship $\propto I_{peak}^{7/9}$ (Fig. 5), which is also characteristic of pressure dependence on laser intensity for ablative sub-critical laser plasmas [21,22]. Third, hot and dense ablative nanosecond laser plasma is known to be responsible for expulsion of multimicron sized droplets through bulk melting and overheating of solid materials at GW/cm^2 laser intensities [3,15,41] and in our plasma imaging studies we observed such melt expulsion at high $I_{peak} \geq 4$ GW/cm^2 [Fig. 6(c)].

Hence, following our experimental findings for this laser intensity range ($I_{peak} \geq I_{plas} \approx 0.25$ GW/cm$^2 > I_{PE}$), one can conclude on formation of dense screening laser plasmas in the corresponding "optically thick" ablative carbon plumes, resulting from intense phase explosion of the near-critical superheated melt on the laser-irradiated graphite surface. It is important to note that the threshold of such near-critical phase explosion, providing the maximum (plateau) removal rate (Fig. 2), coincides with those ones for the maximum mechanical coupling coefficient C_m ($C_m \sim P_S/I_{peak}$) at the break point ($I_{peak} \approx I_{plas}$) in Fig. 5, and low-intensity optical breakdown (plasma ignition) at the high—kbar—pressures in the ablative carbon plumes, as was anticipated earlier [4]. Then, the following gradual decrease of $C_m \propto I_{peak}^{-1/4}$ at higher I_{peak} magnitudes can be related to lower pressure generation efficiency in the near-surface ablative subcritical plasma, almost completely shielding the target surface (Fig. 2).

However, there are still two basic experimental facts, remaining unexplained within the framework of this physical picture. First, there is a strict correlation between the onset of the near-critical phase explosion on the graphite surface, accompanied by the drastic rise of carbon vapor pressure in the dense laser plume, and the succeeding formation of the dense (sub-critical), hot ablative laser plasma. In this work we do observe such correlation, but its physical reasons are unclear. Second, the sub-critical plasma pressure (in this work—the pressure P_S) usually exhibits a trend $\propto I_{peak}^{7/9}$ [22], both for the time-resolved ultrasonic measurements of the compression wave amplitude [42], and time-integrated ballistic measurements of the mechanical momentum supplied by the plasma to the target [10,22]. In contrast, the stronger—slightly super-linear ($\propto I_{peak}^{1.1}$)—dependence $P_{rec}(I_{peak})$ (Fig. 2) observed in this work, may indicate additional effects of an intensity-dependent expansion (pressure application) time or of intensity-dependent dimensions of the extending near-surface ablative subcritical laser plasma (Fig. 6), which is a source of ultrasonic emission at the high laser intensities. Interestingly, one possible important link between the near-critical surface phase explosion and the formation of the subcritical laser plasma, as well as the abovementioned spatiotemporal plasma dynamics, is well-known pressure dependence of optical breakdown thresholds in gases and vapors [11]. In the next section, in order to clarify formation and evolution of the subcritical laser plasma in the ablative plumes with their intensity-dependent variable peak vapor pressures and pronounced vapor pressure gradients, we consider the pressure dependence of laser-induced optical breakdown threshold in gases, which determines the spatial dimensions of the optical breakdown (plasma) and its duration in the near-surface region of the ablative plumes.

IV. DISCUSSION

A. Pressure-dependent threshold of the optical breakdown in laser plume

It is traditionally assumed that optical breakdown in gases occurs through an electron avalanche, driven by heating of free electrons by a strong laser electric field via multiple collisions with gaseous neutral species at a rate ν (inverse Bremsstrahlung absorption) [4,10,11]. The avalanche multiplication of free electrons takes place when their kinetic energy becomes comparable to the first ionization potential J_p of the species, at the time increment τ_{ion}, which is a function of laser intensity and wavelength, as well as of gas thermodynamic parameters (pressure P and temperature T) [4,11]. Then, the development of the electron avalanche is assumed to be terminated (at least, in rarefied gases) by complete gas ionization [$N_e(\infty) \approx N$] after a number of carrier duplications steps with the overall ionization time T_{ion} proportional to the product of τ_{ion} and the natural logarithm of the ratio of the gas density N at the given P and T, and initial electron density $N_e(0)$ {usually, $N_e(0)$ is arbitrarily taken equal to 1 cm^{-3}, i.e., under the normal air conditions—atmospheric gas pressure $P_0 = 1$ bar, $T_0 \approx 300$ K, $N_0 \sim 10^{19}$ cm^{-3} – $T_{ion} \approx 40\tau_{ion}$} [11]. As a result, in this simple model, neglecting diffusion and recombination of free electrons, as well as their attachment to neutral atoms to form negative ions, the breakdown threshold intensity I_{break} is defined as the laser intensity value providing complete ionization of the gas exactly at the end of the heating laser pulse [11]

$$I_{break} = \frac{40\pi c J_p}{\tau_{las} \nu R_e \lambda_{las}^2}\left(1 + \frac{\nu^2}{\omega_{las}^2}\right), \tag{5}$$

where c is the electromagnetic velocity in vacuum, $R_e = e^2/m_e c^2 \approx 3 \times 10^{-15}$ m is the classical radius of electron of the mass m_e and charge e, $\omega_{las} = 2\pi c/\lambda_{las}$ is the laser frequency. At the normal conditions for visible laser wavelengths and nanosecond pulses the term in square brackets in Eq. (5) is ≈ 1, providing wavelength- and pulse-width-dependent optical breakdown thresholds $I_{break,0}$[GW/cm^2] $\sim 10^3/\lambda_{las}^2 \tau_{las}$ with the laser wavelength in microns and pulse

width in nanoseconds [4,11,42]. However, at higher gas pressures the I_{break} value rapidly (as P_0/P) decreases, comparing to the atmospheric pressure threshold $I_{break,0}$, due to more frequent electron-neutral particle collisions and the resulting higher heating rate. This decrease occurs until $\nu(P)$ becomes equal to ω_{las} at certain pressure $P_{min}=P_0[\omega_{las}/\nu(P_0)]$, but then the breakdown threshold starts to increase monotonically as P/P_0 [4,11]. The overall pressure dependence for I_{break} is described as follows [11]:

$$I_{break}(P) = I_{break,0}\left[\frac{P_0}{P} + \frac{P}{P_0}\left(\frac{\nu(P_0)}{\omega_{las}}\right)^2\right], \quad (6)$$

exhibiting the minimum exactly at P_{min}.

Importantly, optical breakdown in ablative plumes in front of solid or liquid targets can be easily distinguished from that one in the ambient air atmosphere, since the plume breakdown intensities are by two or three orders of magnitude lower [4,19]. Despite a number of secondary effects [4], including electron and ion emission from the targets, the increase of the near-surface laser intensity due to the surface reflection, local laser electric field enhancement due to surface roughness, the lower average ionization energy for hot ablation products, the main factor underlying nanosecond laser-induced optical breakdown in vapor plumes, is considered to be high vapor pressure of ablation products (in excess of 10^2 bar) [4]. For the near-critical surface phase explosion, raising the plume pressure to the near-critical pressure magnitudes ($\sim 10^3$ bar), which are favorable for optical breakdown at lower I_{break} [43], the optical breakdown becomes directly related to the phase explosion threshold I_{PE}. Moreover, though the equation of state for the near-critical vapor differs significantly from that of ideal gas ($P \sim NT$), in lieu of a multiphase (vapor-droplet) character of ablation products after the phase explosion [24,44–47], the ideal-gas equation can still be considered as a good approximation to account for the vapor density (pressure) effect on I_{break} under these conditions. In this approximation, for the given plume pressure P the high (near-critical) temperature of the ablation products will shift $I_{break}(P)$ curve to higher pressures by an order of magnitude. Furthermore, the high plume temperature provides the corresponding high initial electron density $N_e(0)$ in the plume ($\sim N \times \exp[-J_p/k_B T_{cr}]$) with a minor contribution of thermionic emission, providing complete ionization [$N_e(\infty) \approx N$] of the plumes in the time period proportional to $(J_p/k_B T_{cr})$. The slightly modified $I_{break}(P)$ dependence for the near-critical dense ablation plumes reads as

$$I_{break}(P,T) = \frac{\pi c J_p}{\tau_{las}\nu(P_0)R_e\lambda_{las}^2}\left(\frac{J_p}{k_B T_{cr}}\right)\left(1 + \frac{\nu(P_0)^2}{\omega_{las}^2}\right) \times \left[\frac{P_0}{P} + \frac{P}{P_0}\left(\frac{\nu(P_0)}{\omega_{las}}\right)^2\right], \quad (7)$$

including all the abovementioned important factors—$(J_p/k_B T_{cr})$, spectral and pressure ones [4,5,10,11], which affect optical breakdown of vapor under near-critical laser-heating conditions.

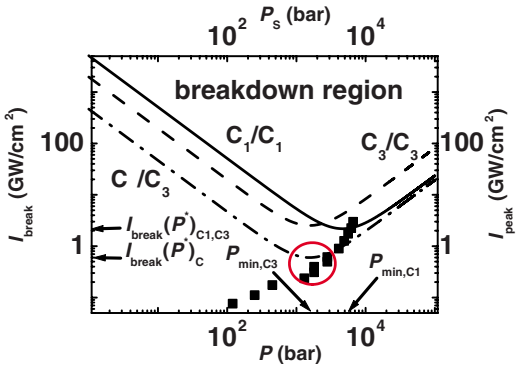

FIG. 7. (Color online) Plume/plasma pressure P_S for $w_0 = 270$ μm (dark squares) versus I_{peak} and the calculated $I_{break}(P)$ dependences for the atomic (continuous curve, ionizing/scattering species—C_1/C_1), small (dashed curve, ionizing/scattering species—C_3/C_3) and large (dotted-dashed curve, ionizing/scattering species—C_∞/C_3) cluster carbon vapor compositions (the calculation details see in the text). The arrows show the calculated breakdown threshold $I_{break}(P^*)$ for C_1,C_3 and C_∞ ionized species, and the pressures $P_{min,C1}$ and $P_{min,C3}$, corresponding to the minimal breakdown thresholds. The circle corresponds to the experimentally observed plasma formation region.

The latter equation was used in this work in calculations of $I_{break}(P)$ values for the employed 25 ns, 532 nm laser pulses, considering, as a zero-order approximation, the near-critical carbon vapor of the atomic (C_1) species [30] with the evaluated collision cross-section $\sigma_{ibs} \approx 1.8 \times 10^{-20}$ m^2 and first ionization potential $J_{p,1} \approx 10.9$ eV [30], and the near-critical phase explosion temperature $\approx 7 \times 10^3$ K [30,31]. The calculated $I_{break}(P)$ curve (Fig. 7) exhibits the minimal I_{break} value of ≈ 2 GW/cm^2 at $P_{min} \approx 4.9 \times 10^3$ bar, in poor agreement with our experimentally observed plasma formation threshold $I_{plas} \approx 0.25$ GW/cm^2 (Figs. 2–6) and corresponding recoil and plume pressures $P_{rec}, P_S \approx 1 \times 10^3$ bar (Figs. 2 and 5) (see two or three orders of magnitude higher I_{break} values measured so far for much lower gas pressures, in Refs. [11,19]). The possible discrepancy between the calculated and measured magnitudes I_{break} and I_{plas}, respectively, by the factor of 10 may result from our experimental uncertainties, e.g., neglecting the intermediate electronically excited species in the carbon plumes, transient surface reflection, thermionic emission, the rather rough estimates for σ_{ibs} related to the rather extensive carbon cluster abundance for the near-critical carbon vapor composition (predominantly, C_1 and C_3 species [48]), as well as from the very approximate character of the ideal gas equation used in the near-critical thermodynamic region (i.e., the vapor density will be higher in the region, approaching to the liquid carbon density [33]). As an example, according to our calculations, the increase of σ_{ibs} to $\approx 5.4 \times 10^{-20}$ m^2 for C_3 species ($J_{p,3} \approx 12$ eV [38]), which are also present (even predominating [48]) in the near-critical region, would yield in much lower and closer $P_{min} \approx 1.6 \times 10^3$ bar, but in almost the same $I_{break} \approx 2.4$ GW/cm^2 (Fig. 7). These results indicate that the variation of the vapor composition affects presumably $\nu(P_0)$ (through σ_{ibs}), significantly changing $P_{min}=P_0[\omega_{las}/\nu(P_0)]$. Apparently, the breakdown threshold I_{break} can be influenced

mostly by changes in J_p (e.g., for large graphitelike carbon nanoclusters C_∞, simultaneously emerging as a significant high-mass fraction of a vapor-droplet mixture of ablation products during such near-critical phase explosions [45–47], their first ionization potential $J_{p,\infty}$ may become as low as the work function of graphite $\approx$4.6 eV [49]), reducing the threshold by the factor of $(J_{p,\infty}/J_{p,1,3})^2 \sim 10$ and the corresponding magnitude P_{min} by the factor of $(J_{p,\infty}/J_{p,1,3}) \sim 3$. However, despite of the reasonable agreement between I_{plas} and I_{break} (Fig. 7), when impact ionization of the high-mass carbon nanoclusters C_∞ is presumably taken in to account, the rather high electron affinity values ($\approx J_{p,\infty}$) for such carbon nanoclusters [49] make them poor scattering partners in electron-neutral collisions due to electronic attachment, so more efficient laser heating of electrons seems to occur in their collisions with the most abundant C_3 species.

Hence, in the lieu of the incomplete agreement between the experimental (I_{plas}) and calculated (I_{break}) breakdown thresholds for low-mass carbon species $C_{1,3}$ ablated from the graphite target, one can suppose the important role of the nanocluster (nanodroplet) fraction of the near-critical phase explosion products during optical breakdown in the ablative carbon plumes [24], among other factors such as electron and ion emission from the target, the increase of the near-surface laser intensity due to the surface reflection, local laser electric field enhancement due to the surface roughness, and the lower average ionization energy for hot ablation products [4]. Similarly, the nanodroplet fraction of the near-critical surface phase explosion products may be responsible for highly nonlinear, spatially inhomogeneous electron avalanche in the ablative plumes prior their plasma ignition, providing the observed stochastic, strongly perturbative spatial structure of the near-surface plasma "opaqueness" region [12] due to the different optical breakdown thresholds for the carbon vapor and nanodroplet plume components.

B. Spatiotemporal dynamics of optical breakdown and plasma in the laser plumes

The correlated drastic increase of $X(I_{peak})$, $P_{rec}(I_{peak})$ and $P_S(I_{peak})$ curves near the phase explosion threshold I_{PE} (Figs. 2, 3, and 5), which represent, respectively, cumulative and instantaneous (peak) parameters of the ablative mass removal, indicates that the latter process occurs continuously during the heating laser pulse with the intensity profile $I(t)$. This fact provides a direct monotonous relationship between magnitudes of the instantaneous vapor pressure $P(t)$ in the near-surface Knudsen layer and instantaneous laser intensity $I(t)$, described in each time instant by some functional form, which can be determined, e.g., using the experimental $P_S(I_{peak})$ dependence. Then, once plotted in Fig. 7, these curves illustrate how the vapor pressure $P(t)$ in the Knudsen layer, rising during the laser pulse versus the instantaneous $I(t)$, at some pulse instant $-t^*$ (the Gaussian $I(t)$ profile has its peak at a zero-time instant) crosses the curve $I_{break}(P)$ in the point $I_{break}(P^*)$, where the carbon vapor with the local pressure P^*, flowing through the near-surface Knudsen layer, undergoes to optical breakdown. If $I(t)$ increases further during the laser pulse, the pressure $P(t)$ of the flowing vapor in this layer rises too (Figs. 2 and 5), supporting more intense optical breakdown (since $I \gg I_{break}$ for $P > P^*$). The optical breakdown occurs in the layer in the new portions of ablation products until the moment $+t^*$ when the vapor pressure and laser intensity fall down to their threshold values P^* and $I_{break}(P^*)$, respectively. Likewise, optical breakdown extends across the laser spot involving the spatial region where the vapor pressure exceeds P^*. Hence, it appears that, in agreement with previous experimental observations [9], for the particular *nanosecond laser ablation* conditions (laser wavelength, pulsewidths, intensity profile) one can derive a case-specific optical breakdown threshold intensity $I_{break}(P^*)$, which determines the onset of plasma formation. The existence of this threshold introduces the initial radius W_{break} of the breakdown plasma for the incident focused Gaussian beam

$$W_{break}(I_{peak}) = w_0 \sqrt{\ln\left(\frac{I_{peak}}{I_{break}(P^*)}\right)} \tag{8}$$

and duration of optical breakdown in the vapor, $T_{break} = 2t^*$, in the explicit form

$$T_{break}(I_{peak}) = \tau_{las} \sqrt{\ln\left(\frac{I_{peak}}{I_{break}(P^*)}\right)}. \tag{9}$$

Such thresholdlike occurrence of the optical breakdown in the near-critical vapor plume may considerably affect the very early formation and expansion stages of the resulting plasma both on spatial and temporal scales, e.g., by defining the initial plasma source dimensions or the pressure application times on the target surface, respectively. In particular, our contact ultrasonic measurements on the rear side of the graphite samples performed by means of the rather slow transducer for the ultrasonic transients considerably broadened in the polycrystalline graphite samples, may be significantly affected by the these effects. Indeed, the slightly super-linear $P_{rec}(I_{peak}) \propto I_{peak}^{1.1}$ curve in Fig. 2, which was obtained under the abovementioned conditions, differs from those obtained via mechanical pendulum measurements ($P_{pend} \propto P_{plas} \propto I_{peak}^{3/4}$) [22,50] by the factor $\{\ln[I_{peak}/I_{break}(P^*)]\}^{1/2}$, while its account in the form $P_{rec} \sim P_{plas}\{\ln[I_{peak}/I_{break}(P^*)]\}^{1/2}$ provides a perfect fit to the experimental curve (Fig. 2). In fact, such region of super-linear increase may be present on all the abovementioned obtained dependences of recoil pressure or mechanical momentum on laser intensity for $I_{peak} \geq I_{PE}$ [22,50], but eventually—on the broad intensity scale—transforms for the saturating factor $\{\ln[I_{peak}/I_{break}(P^*)]\}^{1/2}$ into the pure trend $P_{plas} \propto I_{peak}^{3/4}$ [22,50]. Hence, one can relate the superlinear region of the $P_{rec}(I_{peak})$ curve to the time-integrated character of our ultrasonic measurements with the slow ultrasonic transducer and thick polycrystalline graphite targets, affected by the duration of the plasma pressure application to the target surface (the temporal breakdown threshold factor) $T_{break}(I_{peak})$. Alternatively and more probably, one can consider the similar spatial factor $W_{break}(I_{peak})$, accounting for the effective dimensions of the breakdown region in the near-surface vapor plume as the primary ultrasonic source on the ablated target surface. For the such ambiguity, the enlightening point is the satura-

tion of the $X(I_{peak})$ curve in Fig. 2 for $I_{peak} \geq I_{plas}$ at the monotonously increasing $P_{rec}(I_{peak})$, which demonstrates that the mass removal is terminated in this intensity range and recoil pressure on the target surface is provided by the backward plasma pressure. Effectively, this means that for $I_{peak} \geq I_{plas}$ there is no temporal correspondence between the near-surface vapor pressure and the incident instantaneous laser intensity and the factor $T_{break}(I_{peak})$ is not applicable. In contrast, the surface screening by the dense plume expelled under the near-critical surface phase explosion does not affect extension of optical breakdown across the laser spot, thus bringing up the more relevant spatial factor $W_{break}(I_{peak})$.

In contrast, comparing to the laser spot size w_0, this spatial factor does not affect the initial size of the pressure source in our noncontact air measurements, otherwise, upon correction for the factor, the $P_{air}(I_{peak}) \propto I_{peak}^{4/9}$ curves in Fig. 3 would demonstrate much weaker sub-linear trends. Hitherto, one can conclude on considerable and fast extension of the ablative plasma within the laser spot during the heating laser pulse (Fig. 6) with the resulting lateral plasma radius comparable to w_0, while at the speed exceeding the initial speed ($\sim$1 km/s) of the detected shock waves (Fig. 4) to be insensitive to the factor $W_{break}(I_{peak})$. The latter condition can be readily fulfilled either for intrinsic gas dynamic expansion of the subcritical plasma, or for the plasma extension by means of a laser-supported combustion wave, preheating the surrounding plume or air species via fast electron and/or radiative heat conduction [1,18–20]. Such a wave typically originates near the maximum of C_m [18–20,49] and, thus, in accordance with our findings, from the surface phase explosion near the critical point of carbon. In contrast, similar laser-supported detonation waves of plasma extension at speeds of the order of 10 km/s, driven by preheating of the ablative plumes and ambient air by much faster diverging breakdown-induced strong (GPa-level) shock waves [1], would reveal no influence of the laser waist size w_0, but this is not the case in our work (Fig. 3).

V. CONCLUSIONS

In this work the primary focus was on experimental studies of optical breakdown and plasma ignition in high vapor pressure ablative plumes produced during nanosecond laser ablation of graphite. It was experimentally demonstrated that the breakdown threshold is considerably decreased (down to 0.1–1 GW/cm^2) at high—kbar—vapor pressures, provided in the laser plume via intense quasi-continuous mass removal during the preceding near-critical phase explosion in the superheated molten surface layer of graphite. As a result, the near-critical surface phase explosion yields not only in such intense mass removal and maximum mechanical coupling coefficient, but also in complete shielding of the target surface by the high-mass nanocluster ablation products, and in low-intensity optical breakdown in the high-pressure, high-temperature plume, with all these important phenomena appearing in the correlated manner in the narrow laser intensity range just above the phase explosion threshold. The ablative laser plasma succeeding the optical breakdown in the carbon plumes is identified in the range 0.1–100 GW/cm^2 as subcritical near-surface plasma with the intensity-dependent initial dimensions, the measured pressures up to several GPa, and temperatures up to 10^2 eV evaluated using the well-known scaling relationships for basic plasma parameters. The transient extension of the plasmas during the heating laser pulse was shown to occur in the laser-supported combustion, rather than detonation, wave regime.

ACKNOWLEDGMENTS

The authors acknowledge useful discussions with Dr. Alexander Bulgakov and Dr. Nadezhda Bulgakov (Institute of Thermophysics, SB RAS). This work was supported in part by the Russian Foundation for Basic Research (Projects No. 08-08-00756a and No. 10-08-00941a).

[1] D. Bäuerle, *Laser Processing and Chemistry* (Springer, Berlin, 2000).
[2] A. Miotello and R. Kelly, Appl. Phys. Lett. **67**, 3535 (1995).
[3] N. M. Bulgakova, A. V. Bulgakov, I. M. Bourakov, and N. A. Bulgakova, Appl. Surf. Sci. **197-198**, 96 (2002).
[4] M. M. Martynyuk, Sov. Phys. Tech. Phys. **21**, 430 (1976).
[5] V. I. Luchin, Izv. Vyssh. Uchebn. Zaved., Radiofiz. **23**, 177 (1980).
[6] M. Baudelet, M. Boueri, J. Yu, S. S. Mao, V. Piscitelli, X. Mao, and R. E. Russo, Spectrochim. Acta, Part B **62**, 1329 (2007).
[7] L. B. Brostoff, J. Gonzalez, P. Jett, and R. E. Russo, J. Archaeol. Sci. **36**, 461 (2009).
[8] J. J. Gonzalez, A. Fernandez, D. Oropeza, X. Mao, and R. E. Russo, Spectrochim. Acta, Part B **63**, 277 (2008).
[9] N. G. Basov and O. N. Krokhin, Sov. Phys. JETP **19**, 123 (1964).
[10] J. F. Ready, *Effects of High Power Laser Radiation* (Academic, Orlando, 1971).
[11] N. I. Koroteev and I. L. Shumay, *Physics of High-Power Laser Radiation* (Nauka, Moscow, 1991).
[12] Yu. A. Zakharenkov, O. N. Krokhin, V. V. Pustovalov, V. P. Silin, G. V. Sklizkov, A. N. Starodub, V. T. Tikhonchuk, and A. S. Shikanov, JETP Lett. **23**, 35 (1976) [Pis'ma Zh. Eksp. Teor. Fiz. **23**, 40 (1976)].
[13] N. M. Bulgakova and A. V. Bulgakov, Appl. Phys. A: Mater. Sci. Process. **73**, 199 (2001).
[14] X. L. Mao and R. E. Russo, Appl. Phys. A: Mater. Sci. Process. **64**, 1 (1996).
[15] R. E. Russo, X. L. Mao, H. C. Liu, J. H. Yoo, and S. S. Mao, Appl. Phys. A: Mater. Sci. Process. **69**, S887 (1999).
[16] A. V. Bulgakov and N. M. Bulgakova, Quantum Electron. **29**, 433 (1999).
[17] G. Cristoforetti, G. Lorenzetti, P. A. Benedetti, E. Tognoni, S. Legnaioli, and V. Palleschi, J. Phys. D **42**, 225207 (2009).
[18] R. G. Root, J. Phys. Colloq. **41**, C9-59 (1980).

[19] C. L. M. Ireland and C. G. Morgan, J. Phys. D **7**, L87 (1974); A. Sircar, R. K. Dwivedi, and R. K. Thareja, Appl. Phys. B: Lasers Opt. **63**, 623 (1996).
[20] B. Xu, Q. Wang, X. Zhang, S. Zhao, Y. Xia, L. Mei, X. Wang, and G. Wang, Appl. Phys. B: Lasers Opt. **57**, 277 (1993).
[21] C. R. Phipps, J. R. Luke, T. Lippert, M. Hauer, and A. Wokaun, Appl. Phys. A: Mater. Sci. Process. **79**, 1385 (2004).
[22] C. R. Phipps, T. P. Turner, R. F. Harrison, G. W. York, W. Z. Osborne, G. K. Anderson, X. F. Corlis, L. C. Haynes, H. S. Steele, K. C. Spicochi, and T. R. King, J. Appl. Phys. **64**, 1083 (1988).
[23] S. I. Kudryashov, A. A. Karabutov, and N. B. Zorov, Mendeleev Commun. **8**, 6 (1998).
[24] S. I. Kudryashov, Ph.D. thesis, Moscow State University, 1999.
[25] A. Rohlfing, C. Menzel, L. M. Kukreja, F. Hillenkamp, and K. Dreisewerd, J. Phys. Chem. **107**, 12275 (2003).
[26] S. I. Kudryashov, V. D. Zvorykin, A. A. Ionin, V. Mizeikis, S. Juodkazis, and H. Misawa, Appl. Phys. Lett. **92**, 101916 (2008).
[27] T. Efthimiopoulos, E. Kritsotakis, H. Kiagias, C. Savvakis, and Y. Bertachas, J. Phys. D **31**, 2648 (1998).
[28] S. I. Anisimov, Ya. A. Imas, G. S. Romanov, and Yu. V. Khodyko, *Action of High-Power Laser Radiation on Metals* (Nauka, Moscow, 1970).
[29] T. Venkatesan, D. C. Jacobson, J. M. Gibson, B. S. Elman, G. Braunstein, M. S. Dresselhaus, and G. Dresselhaus, Phys. Rev. Lett. **53**, 360 (1984).
[30] E. I. Asinovskii, A. V. Kirillin, and A. V. Kostanovskii, High Temp. **35**, 716 (1997).
[31] M. A. Sheindlin, Teplofiz. Vys. Temp. **19**, 630 (1981); F. P. Bundy, W. A. Bassett, M. S. Weathers, R. J. Hemley, H. U. Mao, and A. F. Goncharov, Carbon **34**, 141 (1996).
[32] E. Leveugle, D. S. Ivanov, and L. V. Zhigilei, Appl. Phys. A: Mater. Sci. Process. **79**, 1643 (2004).
[33] V. P. Skripov *et al.*, *Thermophysical Properties of Liquids in the Metastable State* (Gordon and Breach, NewYork, 1988); P. G. Debenedetti, *Metastable Liquids: Concepts and Principles* (Princeton University press, Princeton, NJ, 1996).
[34] B. J. Garrison, T. E. Itina, and L. V. Zhigilei, Phys. Rev. E **68**, 041501 (2003).
[35] S. I. Kudryashov, K. Lyon, and S. D. Allen, Phys. Rev. E **75**, 036313 (2007).
[36] I. S. Grigor'ev and E. Z. Meylikhov, *Physical Quantities* (Energoatomizdat, Moscow, 1991).
[37] A. Vogel, J. Noack, G. Hüttmann, and G. Paltauf, Appl. Phys. B: Lasers Opt. **81**, 1015 (2005).
[38] C. Porneala and D. A. Willis, J. Phys. D **42**, 155503 (2009).
[39] Ya. B. Zel'dovich and Yu. P. Raizer, *Physics of Shock Waves and High Temperature Hydrodynamic Phenomena* (Dover, New York, 2002).
[40] O. N. Krokhin, in *Proceedings of the International School of Physics*, edited by H. Knoepfel (Academic Press, New York, 1973), p. 278.
[41] S. Paul, S. I. Kudryashov, K. Lyon, and S. D. Allen, J. Appl. Phys. **101**, 043106 (2007).
[42] S. I. Kudryashov and V. D. Zvorykin, Phys. Rev. E **78**, 036404 (2008).
[43] Y. P. Raizer, *Gas Discharge Physics* (Springer, Berlin, 1991).
[44] X. Fan, M. W. Little, and K. K. Murray, Appl. Surf. Sci. **255**, 1699 (2008).
[45] S. I. Kudryashov, S. G. Ionov, and N. B. Zorov, High Energy Chem. **34**, 101 (2000).
[46] F. Kokai, K. Takahashi, D. Kasuya, A. Nakayama, Y. Koga, M. Yudasaka, and S. Iijima, Appl. Phys. A: Mater. Sci. Process. **77**, 69 (2003).
[47] L. Landström, Zs. Márton, M. Boman, and P. Heszler, Appl. Phys. A: Mater. Sci. Process. **79**, 537 (2004).
[48] In our recent time-of-flight mass spectroscopy experiments under the same conditions we observed almost equal uncorrected abundances of C_1 and C_3 neutral species under such near-critical laser-induced phase explosion conditions, but the latter should be corrected to the $3^{1/2}$ times lower ion-electron conversion efficiency for the heavier clusters. Simultaneously, larger neutral carbon clusters (C_5-C_{27}) appearing in mass-spectra with much lower abundances are known to be condensation products of the smaller ones.
[49] S. I. Kudryashov, N. B. Zorov, and S. G. Ionov, Mendeleev Commun. **9**, 61 (1999).
[50] D. W. Gregg and S. J. Thomas, J. Appl. Phys. **37**, 2787 (1966).